Measurement & Instrumentation Systems
National Space Institute
Technical University of Denmark

,

Micro Advanced Stellar Compass
General Information

Prepared for:

Prepared by: Space Instrumentation Group

Issued by: V. Tauber-Møller

Approved by: P. S. Jørgensen

Ref.: ASC-DTU-PRP-3000 Issue 1.3

Date: December 19, 2012

Change Record

Version	Date	Changed paragraphs	Remarks	Author
1.0	09 May, 2006		New Release	R. Michelsen
1.1	14 December, 2006	All	Misc. typographical corrections	R. Michelsen
1.2	28 April, 2010	All	Edit language and update layout	D. Mechlenborg
1.3	19 December, 2012	All	Edit language and update layout	V. Tauber-Møller

Table of Contents

1 Introduction

The Space Instrumentation Group (SIG) under the section for Measurement & Instrumentation Systems (MIS) at the National Space Institute (NSI) of the Technical University of Denmark (DTU) has extensive experience and heritage in designing, developing, producing, and testing autonomous and advanced star sensors.

This document contains a technical description of the micro Advanced Stellar Compass (microASC). More specifically it addresses the following topics:

- Description of the design
- Performance, functionality, and operations
- Interfaces and budgets
- Calibration and verification
- Ground support equipment
- Other features

The microASC is the latest generation of the Advanced Stellar Compass (ASC), and from the ASC the microASC inherits the science part of the software, as well as the technology and methodology to select and to qualify the components and the instrument for use in space. The microDPU has successfully passed all qualification tests. The CHUs are similar to the type used on the ASC, which has considerable flight heritage.

The ASC has been procured by 20 projects for a total of 26 DPUs and 33 CHUs, of which 25 DPUs and 32 CHUs have been launched. All the major space Agencies (ESA, CNES, NASA, DLR, JAXA) have acquired the ASC and the projects span all classes up to the cornerstone-type of mission, e.g. the ESA Earth Observation Mission GOCE.

To date the accumulated flight time of the ASC is in excess of 95/202 years (DPU/CHU respectively).

The main microASC design goal is to inherit as much of the ASC instrument as possible while still allowing for improvements to augment the performance envelope. Since the target CPUs are of the same family, it has been possible to adopt 95% of the flight-proven ASC software directly, including the core centroiding and pattern matching functions. This is of high value, when the performance criteria are to be established, especially in non-nominal configurations. These configurations are usually difficult to simulate on-ground. Therefore past experience in space, which can be directly applied, is highly valuable. Further, the design of the ASC CHU has been transferred to the microASC, thus providing substantial flight heritage to the microASC design.

The first microASC was successfully launched in 2008 and has operated successfully since then. The microASC has by now accumulated 43 years flight heritage and currently 23 microASC instruments are flying in space, including NASA, ESA, CNES, and JAXA missions. More than 55 microASC instruments have been delivered to their respective projects, e.g. NASA's Juno mission and ESA's Swarm mission.

The ASC and the microASC have been subjected to many very different orbital and thermal environments, and not a single hardware or functional failure has occurred despite being exposed to the heavy solar storms that occurred during the solar flares maximum period.

It is also worth to note that the instruments are flying on different orbits - ranging from LEO, over GTO to lunar orbits onboard the ESA/SMART-1 spacecraft - over a large thermal environment envelope, and all the instruments have been subjected to the heavy solar storms that happened at the peak of the solar max phase, during which full operations were maintained. Furthermore, post-launch support has always been given to the full satisfaction of the customers.

The Space Instrumentation Group at MIS, DTU SPACE has the capability and experience to handle several projects simultaneously. To date up to twelve concurrent projects, with widely different requirements, have been handled efficiently with full customer satisfaction.

2 Documents

2.1 Applicable documents

AD 1. -

2.2 Referenced documents

RD 1. -

3 Description of the Instrument

3.1 Configuration

The microASC instrument consists of separate units: one to four Camera Head Units (CHUs) and a micro Data Processing Unit (microDPU). Each CHU is connected by *pigtail* cable to the microDPU. The microDPU can be provided as either a single or a double unit, where the double microDPU is internally fully redundant (Figure 1).

The reasons for the division between the CHU and the microDPU are numerous, but the most important are:

- The CHU can be manufactured to impose very low magnetic disturbance;
- The CHU is very light, 260g including the standard 30kRad shielding, excluding the baffle, hence, it can be located close to the instruments requiring the highest attitude accuracy, e.g. on an optical bench;
- The highest performance of the photo-sensitive sensor of the CHU, the CCD chip, is achieved with a low operating temperature. Using a carefully selected thermal design strategy, the performance of the low power-dissipating CHU can thus be maximized without introducing active cooling;
- The use of more than one CHU is desirable, amongst others, to reduce the operational constraints, like Sun in the field-of-view, and to increase the performance;
- The number of microDPU's and CHUs can be optimized to achieve the highest reliability and availability yet minimizing the mass, volume and power consumption. Consequently, at system level, the architecture is simplified;
- Through the double microDPU, the microASC exists as a fully redundant design and can operate several CHUs. Hence, the reliability of the star sensor, as a whole, considerably increases together with the availability of valid data, with little concern about the operational constraints.
-

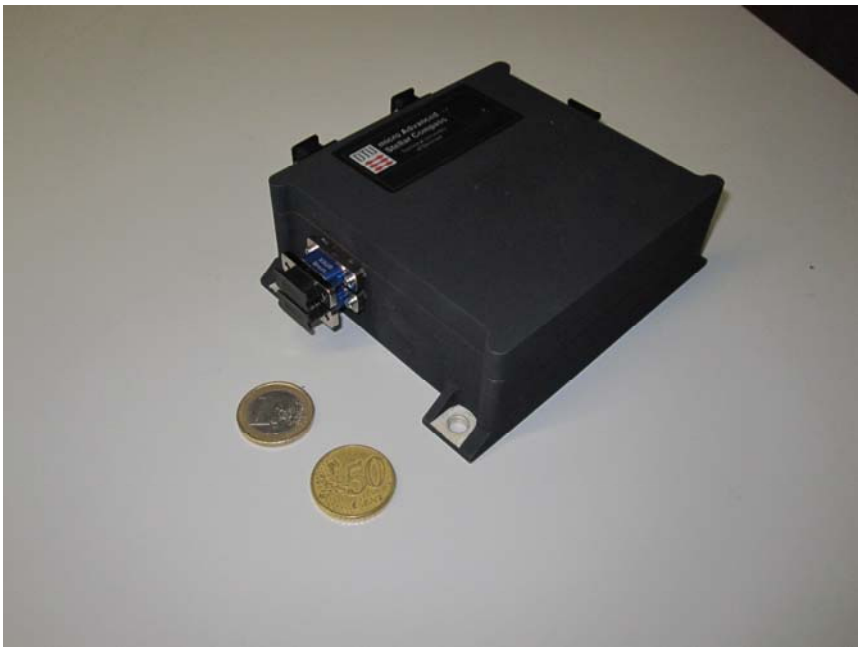

Figure 1: The double microDPU features two fully hot cold redundant Data Processing Units

3.2 Standard Configuration

In order to be able to support different configurations while maintaining the highest degree of commonality and reducing the qualification effort, the microDPU is designed, manufactured, and tested to run one or more CHUs.

The optimal configuration of the microASC depends highly on the mission needs. The needs may focus on accuracy, reliability, flexibility, mission scenario (thermal issues and blinding occurrences) etc.

It should be noted that a configuration with the double microDPU and one to four CHUs not only addresses the basic accuracy and reliability needs, but also provides a tremendous flexibility, e.g. allowing an in-flight re-configuration of which CHUs are operated by each side of the double microDPU. Further, such a configuration supports highly complex attitude manoeuvres, and can be of value for improved support of the AOCS and the payload instrumentation.

3.3 Spare philosophy

All spare parts (PCB, optics, components, etc.) are kept in stock at DTU in order to perform repairs with minimum impact on schedule. Thus it is proposed that spare parts are only provided to the project in case of repairs.

An EM single DPU unit is available on loan basis, as agreed contractually.

3.4 Radiation impact

3.4.1 Radiation Impact Behavioural Model

Based on comprehensive accelerator tests of flight lot parts, and verified in-flight by the results of the radiation impact to the ASC instruments, e.g. onboard the SMART1 Lunar mission spacecraft, a model of the radiation impact build-up has been calibrated and verified. SMART1 used an ion-engine to slowly raise the orbit from GTO to a 300X3000km Lunar orbit. The trajectory encompassed a slow spiral out of the radiation belts, and numerous Corona Mass Ejections were encountered both during the Van Allen belt passages and in deep space. The operations achieved onboard SMART1 therefore forms an excellent platform to validate the performance level achievable for all mission phases based on an analytical model approach.

From images downloaded from devices under energetic baryon bombardment in an accelerator, cross sections, threshold energies, and expressivities for the various radiation impact phenomena have been established, as a function of impacting particle and energy.

From images downloaded from the SMART1 spacecraft, the expressivity of the accumulated radiation impacts versus CCD temperature has been generated and verified. And from images acquired during passage of the Van Allen proton belts, as well as from the achieved attitude accuracy and availability, another expressivity model for the impact of energetic protons has been established and calibrated. The validation by in-flight measurements augments the model by also ensuring that it encompass both multi energetic irradiation as well as omnidirectional impacts.

The expressivity models thus arrived at, are used to predict performance figures for a given future mission, with high fidelity, and to determine the operational margins at various mission phases, including the performance under massive corona mass ejections (CMEs) and EOL.

These models can be used to generate the performance predictions once the specific orbit and radiation environment is known.

3.4.2 Radiation environment impact assessment

Detailed considerations on the influence from the radiation environment will have to be based on further information on the mission, its scenarios, and orbits.

As an example, the radiation analysis typically results in that the standard shielding is appropriate for LEO, GEO, and deep space missions, whereas missions encompassing phases, where the equipment will have to spend extended time inside the radiation belts, will have to use the augmented shielded units.

3.5 Gravity Model

The microASC instrument already exists. Therefore the gravity model has been constructed from existing models.

3.6 Principle of Operation

The microASC has been developed as a fully autonomous star tracker, including all brighter stars within the camera Field Of View (FOV) in the attitude solution. Furthermore, the instrument has been optimized towards supplying the highest possible overall attitude accuracy for the spacecraft. This has been achieved by splitting the instrument into a Camera Head Unit (CHU) and a Data Processing Unit (microDPU), which may be separated by more than 20m.

Because each CHU dissipates only 0.27W, and its mass is approximately 260g, the CHU can be placed close to the instrument that sets the highest attitude requirements. Furthermore, the thermal dissipation and the thermal radiation to space through the lens is arranged to ensure full performance without active thermal control (Peltier coolers/heaters) for most mission profiles.

The microDPU can drive up to four CHUs at a user selectable update rate up to 32 updates per second (for four CHUs).

After the microDPU gains access to the acquired image, it analyses the star positions to calculate the inertial direction of the boresight and the rotation about this axis, in combination referred to as the attitude. These coordinates are then transformed to a user defined spacecraft coordinate system, and are output in the form of quaternions.

The image analysis functions performed on an image depend on several conditions. In normal operation, the angular difference between two consecutive images is so small that the following procedure is adequate. The image is sifted for stars. All detected stars are warped and their positions are calculated with hyperacuity. Based on the previous attitude and the star catalogue, a star image is formed. The two images are then matched. Based on this match, the relativistic attitude is found. This attitude is then corrected for astronomical aberration and output to the telemetry queue.

In a number of situations no attitude history exists, for example after a power cycling or following a CHU blinding. In such cases an extra image processing step, initial attitude acquisition, is included: The hyperacuity star positions are analyzed for triplets of nearest and next nearest neighbors. The resulting set of triplets is then matched to a preflight-compiled version of the star catalogue called the star database. The entries in this star database are all conceivable triplets. Based on this match a crude attitude is obtained. This crude attitude is then used as a seed, instead of the previous invalid attitude, in the consecutive processing.

In order to transform the relativistic attitude to heliocentric attitude, the velocity vector of the spacecraft relative to the heliocentric system is needed. This vector is obtained via the day of year and an orbit model. The orbit model needs to be updated at intervals from hours to days depending on the orbit-perturbing forces (air-drag). Typically, these updates are based on GPS data. The correction amounts to maximum 26 arcsecond for LEO.

Apart from the attitude determination, the software maintains a list of other functions, which may be divided into the following three categories:

1. Communication functions: An I/O queue for TM and TC. A dedicated debug-line for monitoring and closed-loop testing. System and housekeeping monitoring.
2. Supervisory functions: An SW-watchdog monitors the task switching and program execution. A hot-spot database that monitors the ageing and occasional radiation damages of the CCD-chip. A bit-washing function refreshing the EDAC-protected memory at user-specified intervals.
3. Imaging functions: Automatic or user specified image acquisition, compression, and TM. A planetary feature-tracking module. Non-stellar-object detection.

3.7 Hardware description

3.7.1 The microDPU

The microDPU is a miniature data processing unit that implements all the functionality for an extremely fast and robust attitude determination. The microDPU comes as either a single or a double sided unit. Physically, the double microDPU is split into five boards in a cold/hot redundant configuration. Each redundant side consist of a processor board and a power supply board. The last board is a cross strapping board that allow for a fully flexible drive of the attached one to four CHUs to any of the two redundant processors. By adopting two parallel power/processor systems, all sources for single point failures are thus effectively removed.

Each CPU board is equipped with a processor, 8MB full EDAC SDRAM, 8MB full EDAC FLASH memory, a boot prom, pipeline structure and glue-logic in FPGA, and communication ports.

The power supply board consist of a fully isolated, high efficiency SEL immune DC/DC stage, power filters, distributed latch-up sense and handling blocks, and power switching circuitry.

The cross strapping board is a switch board that directs power from the active side to the enabled CHUs, and receives and gates the data to the same side. The redundant side may be inactive or active, as requested, and may drive the CHUs not used by the other unit. The user may at any time select which CHUs are assigned to which redundant side.

The microDPU is equipped with eight MDM connectors: two for power input, two for communication and four for connection to the four CHUs.

3.7.2 The CCD CHU

Each of the four CCD CHUs (Figure 2 and 3) consist of a powerful optical system, mechanical support structure, radiation shielding and the CCD and associated support electronics. The support electronics includes HK-sensors, sequencer and drive level electronics, CDS system and line amplifier for the up to 20m signal line to the microDPU. The CHU design has substantial flight heritage, and is the same design as flown on the ESA SMART-1 mission to the Moon. The CHU has thermal and radiation wise proven to be extremely robust, so that in combination with the microDPU it provides valid attitudes even when situated in the Earth radiation belts under the harshest, worst case solar storms.

Figure 2: The Camera Head Unit

3.8 Software Description

3.8.1 Architecture

3.8.1.1 System Partitioning

The software of the microASC is partitioned into sub-modules each having a specific task and clear interfaces. The modules have been organized to minimize mutual interface complexity, resulting in a number of qualities in all system phases, e.g.:

- Software visibility is increased for the customer.
- Each module can be/and is verified and validated separately.
- Possibility of modifying software modules separately.

The modules are divided into two different classes: Hard and soft modules.

The hard modules are stored in ROM. These modules form the safe mode of the instrument that can be entered during system startup. All core system functions can be accomplished during the safe mode, such as memory uploading, change of runtime parameters and house keeping of the instrument. The functions that can be performed in the safe mode are a subset of the functions, which can be performed in normal operations mode. The intention of the safe mode is to provide a mode where uploading of software can be performed if a contingency should render the normal software from being loaded. This situation is, however, not expected to happen, and has never been detected during flight. The modules that form the safe mode are:

- Core operating system
- Core telecommand dispatching/scheduling

Core signifies that only the subset of the functions from application mode needed for safe mode is implemented.
The soft modules of the microASC software are stored in FLASH type memory. These modules comprise the application (normal) mode of the system and can easily be modified on ground as well as in flight. The modules are:

- Operating system: Interrupt handling, access to shared resources
- Telecommand handling: Dispatching, scheduling, execution, production of telemetry
- System parameter module
- Centroiding module
- Pattern matching module
- Star database
- Star catalogue

Discrepancies in operational environment between ground estimations and actual flight conditions may surface. Examples of such discrepancies include: Interface temperatures being outside the operational range; spacecraft appendages being inside or close to the CHU FOV, optical misalignments caused by shifts in spacecraft structure from launch load and gravity release, etc. Such contingencies are characterized as being unforeseen for all parties. In most situations the contingencies can be circumvented by a software modification and the microASC can be brought back to almost 100% operation.

3.8.1.2 Parameterization

Apart from the full module uploading, the operation of the microASC can be trimmed by uploading runtime parameters to the system. These parameters cover a wide spectrum of the runtime operation such as sensitivity, alignment, protection settings, integration time, and can be uploaded separately. This class of telemetry gives a non-critical, extremely easy way of optimizing performance in space. The size of telemetry packets used for parameter changes is in the range of 20 bytes.

3.8.1.3 Observability/Traceability

The attitude telemetry includes, in addition to the determined attitude, information of each step of this attitude determination. If the microASC fails to determine an attitude, the cause can be derived from this information, e.g. camera blinding.

3.8.1.4 Resource Budgets

The resource usage has been analysed with respect to memory usage and CPU load.

The memory usage analysis covers the usage of the runtime stack and concludes that the most memory consuming paths in parallel do not exceed 50% of the total stack size. It should also be noted that no recursive functions are used in the microASC software.

The CPU load is determined by test by measuring the time that the CPU spends in idle state pr. unit time. Tests under nominal conditions have showed that 32 images can be handled each second. Support of e.g. 4 CHUs at 250ms integration time (16 images/s) will therefore, under nominal conditions, result in a CPU load of 35%.

3.8.2 Software verification and Validation

The function, operation, and performance of the above-mentioned software functions are thoroughly evaluated in full accordance with the ECSS guidelines. The instrument performance is further assessed at unit level using the below mentioned tests.

The star tracking robustness is assessed by real-sky tests with the CHU pointing at specific areas of the night-sky. The performance is tested in areas, which, based on simulations, are known to present worst case conditions for the instrument, either due to stellar distributions far from the average, or to excessive numbers of false stellar objects, such as galaxies, planets, the Moon, or satellites. The code has hereby proven to operate nominally and to yield yielding a recovery from a lost-in-space condition on the entire night-sky. By adding artificial noise-objects to the image prior to the analysis, it was proven that the algorithms may handle a substantial number of false objects without noticeable performance degradation.

The star tracking accuracy is established partly via real-sky tests and partly via controlled laboratory tests. During the real sky test, the instrument relative accuracy is relocated to an astronomical site to reduce atmospheric dimming and refraction effects. Performance is assessed in both rich and meagre star fields which represents the two worst case conditions at hand (accuracy versus CPU usage). During the laboratory tests, the instrument noise equivalent angle accuracy is assessed versus temperature. Combination of the two assessment techniques offers a unique method of projecting the in-flight accuracy. Post launch assessments have always demonstrated a good correlation to the pre-flight predictions.

The star tracking timeliness is established from real sky testing, where the attitude latency (time duration from center of integration to attitude output) is measured under worst case conditions.

All software components are implemented in-house leading to a number of advantages:

- Full visibility of the software.
- If any modifications (e.g. in the protocol layer) should be performed, the customer interacts directly with the programmer instead of through a third party.
- Validation and verification can be performed to fit the customer's standards /requirements.

3.8.3 Software Protection Mechanisms

The microASC S/W has several built-in protection mechanisms, in order to ensure the high performance. These mechanisms are implemented mainly with radiation effects in mind. If an undetermined software state is entered due to radiation, it should be noted that the microASC is designed in such a way that no action from the CPU can harm or be hazardous to the hardware of the microASC in any way, even for a prolonged period of time.

3.8.3.1 Police Program and Watchdog

The police program and the watchdog are protection mechanisms that ensure the software program has not entered an infinite loop. Such loops can be created from undetected RAM bit-flips due to radiation.

The watchdog program is a low-level hardware watchdog that controls the software interrupt level. It is reset by the timer interrupt and the hardware will automatically force an instrument reboot if the watchdog is not reset.

The police program is an application layer watchdog, reset each time the scheduler switches to a new task. The program is controlled from the timer interrupt that forces an instrument restart if the program is not reset.

Together, the watchdog and the police program form a complete protection mechanism of stale loops and corrupted interrupt structures.

3.8.3.2 Error Detection and Correction on FLASH Memory and RAM Memory

The soft modules that can be uploaded are all stored in FLASH type memory. This memory segment, like the RAM segment, is protected with Error Correcting Code (ECC) with a minimum distance of 4, which means that single bit-flips can be corrected and double bit-flips can be detected (within a 16 bit word). If a bit-flip should occur due to radiation, it will be detected the next time it is read and corrected immediately. It should be noted that no FLASH bit-flips have yet been detected in space.

3.8.3.3 Bitwash Program

The bitwash program is a loop that can be scheduled to perform a complete read of the memory as a background task, while the microASC is in attitude mode. If any bit-flips have occurred, they will be detected and corrected immediately.

3.8.3.4 Protected Mode CPU Operation

The CPU is operated in protected mode, allowing subprograms to be operated within a contained memory space. This feature increases the detectability of potential untrapped bitflips (inside the EDAC firewall), when subprograms address memory outside their individual address range.

3.9 Functionality and Operations

3.9.1 Functional Characteristics

The microASC is a very versatile instrument, which offers several functions to the user:

- Autonomous attitude determination from *lost in space* in less than 80 msec;
- Highly Accurate attitude determination;
- Possibility to output the attitude w.r.t. a user defined reference frame;
- Acquisition of images and image sequences;
- Transmission of images using different compression methods;
- Use of standard telemetry packets (ECSS and CCSDS compatible);
- Highly sophisticated autonomy, including protection mechanisms and automatic system gain setting;
- Fast autonomous recovery from optical overloading;
- Possibility to override all the autonomy, or part of it, by TC either from the spacecraft or from ground;
- Monitoring of the full status of the instrument;
- Possibility of adjusting all the on-board parameters during flight. This can be done autonomously or from ground;
- Possibility to re-program the entire instrument during flight from ground;
- Autonomous single-multiple CHU operation switching;
- Autonomous detection and recovery of SEU, SEL, program flow or stuck operations.

3.9.2 Modes of Operation

The microASC can operate in a number of different modes, which can be entered by telecommand. These modes cover modes for on-ground AOCS testing and characterization as well as in-flight operational modes. In order to be able to test the microASC in conjunction with other instruments (AOCS testing), the microASC has been built with two serial ports; a primary and a secondary data port. The microASC is fully controllable via both communication ports, making simulation mode possible in close loop testing.

3.9.2.1 Safe Mode

The previously described core loader mode, which can be used to upload all or part of the system software, determines instrument health, dumps and checks memory, as well as manages system parameters.

3.9.2.2 Standby Mode

In this mode the microASC does not determine attitudes. This mode can be used for full bandwidth image download, full bandwidth memory download, health monitoring, etc. The attitude mode can be commanded from standby mode, such that attitude telemetry is outputted within 1 sec.

3.9.2.3 Attitude Mode

The normal mode of operation of the microASC is attitude mode. In this mode the attitude is autonomously determined up to 32 times/sec for four CHUs dependent on configuration and parameter setting. The attitude telemetry is either output autonomously or upon request. The

preferred mode of operation is autonomously output, since this will minimize the latency from centre of integration to telemetry output.

3.9.2.4 Simulation Mode

A mode used for on-ground testing, either at unit level, AOCS open loop, or AOCS closed loop testing. A drift around the 3 main axes and an initial direction is uploaded via telecommand. Whenever the pattern matching algorithm receives a centroid list from the centroider to perform pattern matching, the centroids are replaced with the star catalogue positions at the requested direction instead. Noise is added to the centroids, matching the noise of the centroiding algorithm. The acquisition of the centroid positions from the catalogue takes only a few milliseconds, thus this mode simulates the operation in space with respect to performance, latency, and noise. It is therefore an extremely powerful tool for ground testing.

3.9.2.5 Test Image Mode

In this mode, the images acquired by the CHU's are exchanged with an image previously uploaded to a dedicated space in FLASH memory. This mode should only be used during ground testing of the microASC at unit level and at AOCS open loop testing.

3.9.2.6 Stimulator Teach

Another powerful tool for ground testing is the optical Star Field Stimulator (SFS) a type of optical ground support equipment (OGSE). An SFS is a small tube that attaches to the baffle aperture containing typically 3 collimaters, each projecting 3 stars onto the lens. An SFS acts as an artificial night sky and can be moved and turned in order to simulate spacecraft maneuvers. When the teach-in telecommand is sent, the obtained centroids from the centroider are injected into the star catalogue and database (in RAM) at a selected direction. When the centroids are found in the following images (including centroider noise), they can be found and recognized in the selected direction. The SFS is used in conjunction with ground testing at all levels, AOCS open and closed loop testing, noise estimation, polarity verification, etc.

3.9.3 Features

3.9.3.1 Full Autonomy

The microASC is a fully autonomous and carefree instrument. There is no planned maintenance action that must be performed after launch. When the instrument is turned on, it will automatically enter full operational attitude mode in only 5 seconds. After sun blinding of the CHUs, the system will automatically recover after a few seconds. When the radiation dose has accumulated over the lifetime, the system will automatically deal with the associated effects, etc. However, part or all of this autonomy can be disabled from ground.

3.9.3.2 Image Acquisition

The images used for attitude determination can be sent to ground in different formats. This feature can be used either as a background task during attitude determination or as a primary task in standby mode.

3.9.3.3 Raw Format

In this format the image is sent as the raw uncompressed image pixels.

3.9.3.4 JPEG Format

The microASC software includes a JPEG image compressor that can perform lossy compression of the images. The images will lose some details, but the size of the image can be minimized to a few tens of kilobytes.

3.9.3.5 Region of Interest Format

The Region of Interest (ROI) compression technique sends only the image data that is close to the objects in the image. This data is sent in an uncompressed format. The compression factor depends of the number of centroids (40 times when 40 centroids have been found).

3.9.3.6 Centroid List

The centroid list compression is a list of the position and the intensity of all centroids in the image. The compression factor using this format is obviously extremely large.

3.9.3.7 Non-Stellar Object List

This format is very similar to the centroid format, except that all centroids recognized as stars have been removed from the list. Further, the list is augmented with apparent positions in right-ascension and declination of the objects. This feature can be used to track non-stellar objects such as planets, comets, or other satellites.

3.9.3.8 Time Synchronization

The microASC computer has an internal timer, which can be synchronized with the on-board time. It has a resolution of 1µs. However, in order to hold the time stamp in 6 bytes (4 bytes

coarse and 2 bytes fine) a resolution on 15µs is applied in the telemetry timestamping and the time synchronization.
The time synchronization mechanism is very versatile and offer great flexibility in the operation. It may be carried out as shown below:

1. A pulse is sent on one of the dedicated time pulse lines.
2. Shortly after (100µs < t < 900ms), a telecommand indicating the time at the occurrence of the pulse is sent on one of the data lines.

Alternatively, the microASC may date all telemetry in local time, and correlation telemetry packets between the local and the on-board time can be requested by telecommand. Finally, the order between pulse and telecommand can be interchanged.

3.9.3.9 Corrections

The attitude output can automatically be corrected for a number of effects.

3.9.3.10 Annual Aberration Correction

The annual aberration is the relativistic shift of the apparent position of a star on the night sky, caused by the rotation of the Earth around the Sun. If the microASC is supplied with the current date, the attitude output can be corrected for this effect. If not corrected for, the attitude shift originating from this effect is worst case 20 arcseconds.

3.9.3.11 Orbital Aberration Correction

The orbital aberration is the relativistic shift of the apparent position of a star on the night sky, caused by the rotation of the spacecraft around the Earth. If the microASC is supplied with position and velocity of the spacecraft and a date, this effect can be automatically corrected for. If not corrected for, the worst case impact of this effect is approx. 5 arcseconds depending on orbit and attitude profile.

3.9.3.12 Precession Correction

If the attitude must be output in Earth Centered coordinates instead of J2000 coordinates, the attitude output must be corrected for the precession of the Earth. This correction can be made, if the date is uploaded to the system.

3.9.3.13 Nutation Correction

As with the precession of the Earth, the nutation can be corrected for as well, when the attitude solutions must be output in Earth centered coordinates. In order to perform the nutation correction, the microASC must be supplied with the date as well.

3.9.3.13.1 Correction Summary

The table below shows what attitude correction can be performed, and what inputs are needed:

Correction	Date	Position/ Velocity
Annual aberration	X	
Orbital aberration	X	X
Precession	X	
Nutation	X	

3.9.3.14 Non Stellar Object detection and discrimination

When other satellites, comets, asteroids etc. are inside the FOV, they may be incorrectly detected as non stellar objects (NSO). This situation has been investigated and simulated thoroughly. The on-board algorithms are designed to cope with this situation, and it does not induce any performance degradation – even for a very high number of NSOs present.

3.9.3.15 Hot spot rejection

Over the flight time radiation will hit the CCD chip and generate permanent bright spots on the image referred to as hotspots. These spots mimic stars and are detected by the centroiding algorithm as such. The hotspots remains at the same place (same pixel) in the image. Therefore, the microASC carries a hot spot rejection filter, which eliminates them before the pattern recognition is performed. Similarly, a particle transient filter is efficiently rejecting (the much more frequent) dynamic effects from fast baryons passing the sensors active area.

3.9.3.16 House Keeping

The house keeping of the instrument provides information on the system status such as temperatures, video voltages, and the current operational mode. This telemetry can be sent either autonomously or by request. The output frequency can be adjusted by a system parameter.

3.9.3.17 Optional Reference Frame

The microASC will nominally output the calculated attitudes relative to the individual reference frames of the CHUs. This reference frame can be changed to match any desired reference frame, such as the spacecraft frame, the frame of other science instruments, or the frame of the alignment cube of the CHUs. The desired reference frame is adjustable by system parameters and may be trimmed in-flight.

3.9.3.18 Sun exposure

Because most spacecraft cannot guarantee that the star tracker is pointed away from the sun at all times, it is important that the tracker is capable of handling direct sun exposure without being permanently damaged. Therefore, the microASC optics and detector assembly are designed in such a way that direct solar illumination, even for prolonged periods of time,

does not damage the unit. The solar illumination immunity is achieved by assuring that the irradiated solar power is less than the maximum rating of the detector, by including an IR and UV block in the lens coating, and by controlling the point spread function of the lens in such a way, that the power density in the solar spot is so low, that no local heating takes place.

Obviously, star tracking with the Sun inside or near the Field Of View will preclude proper operation of the tracker, because the detector will be brought into saturation. Also, the solar power dissipated in the detector will give rise to a heating of the entire chip. This heating can, if the exposure is of a very long period of time (e.g. days), bring the detector temperature above the maximum limit for full operation, hence a cooling time may be planned for in these cases. Otherwise, a couple of integration cycles, i.e. 0.5s with an integration time of 0.25s, are sufficient to recover nominal operations after the optical overload.

Proper operation of this design has been verified both by the Ørsted and the CHAMP cameras. The Ørsted camera has, intermittently, been directly sun pointing for more than two months in flight. The CHAMP cameras were, periodically, directly sun pointing for more than a week at a time.

3.9.3.19 Earth and Moon exposure

The instrument will automatically isolate and reject non-stellar object detected in the FOV. This is also the case for larger luminous objects, like the Moon and the Earth, as long as the objects do not saturate the CCD.

The Moon will saturate the CCD for lunar phases above 75% when it is within 7° of the central area. For lunar phases below 75%, the attitude robustness will not be impacted.

The dark Earth limb will not lead to saturation of the CCD. The limb may reach all the way to the center of the CCD without impacting the attitude robustness.

The bright Earth limb will lead to saturation of the CCD when approaching the FOV. The exclusion zone depends on the baffle design, but is typically around 20° from the boresight.

Note that for all Moon and Earth intrusions, the attitude accuracy will be lower due to occlusion of stars, and the attitude may be biased due to uneven background. The accuracy estimate and uneven background state are telemetered as parts of the attitude solution.

3.9.3.20 Miscellanea

The centroid determination algorithm and the attitude determination SW have been designed to accept substantial motion smear or attitude rate.
The attitude determination SW is able to handle a substantial number of anomalies, like hot spots, missing stars, or the presence in the image of several non-stellar objects. Upon request, the position of the non-stellar objects can be reported to the S/C or to ground, thus enabling to track them. Both ground tests and flight data show that the presence of planets, say Jupiter, in the field of view of the CHU does not reduce the performance of the microASC.

During power up, the computer performs an extensive integrity check-up. This test includes RAM and ROM checks, SW integrity, CHU temperature, dark current, gain and fixed-pattern-noise, register, interrupt and discrete command status. Discrepancies in the expected system-health are written up in the power on report package.

3.9.4 Detection limit

The detection limit is set at m v = 6.5, but it can be set by the user up anywhere between mv 3 and mv 7.

3.9.5 In flight control

3.9.5.1 Software upload

The microASC software can be uploaded in flight either totally or partially. The upload procedure is, by design, guaranteed to be free from lock-up, and SW uploads may be aborted and resumed at any time.

The FLASH memory has room for several versions of the software, and offers the possibility of determining the present software version by simple system parameter changes. It is therefore possible to upload a new candidate software version, assessing the performance, and reverting to the former version, if the functionality of the updated software version do not meet expectations.

3.9.5.2 In-flight parameters adjustment

The extensive set of parameters of the microASC can be set in-flight directly by a TC. This feature gives the user full control over all autonomous processes, by implementing an easy override mechanism.

3.9.6 Protection mechanisms

3.9.6.1 Latch up protection

Irradiation by energetic particle, and especially baryons, of a microcircuit may result in a host of detrimental effects, the most severe of which being latch-ups. Latch-ups may take many forms, varying from benign stale states of a digital logic, caused by a small part of the circuit logic being shorted out by a funnel created by the ionization trail from the passing particle, to destructive latch-ups where the funnel happens to connect the power plane with ground. In both cases, the latch-up will exist as long as the funnel is kept open. The funnel is in the first place generated by ionizations of the normally isolating silicon between high doped structures, and will normally reset itself within the relaxation time of the technology used, i.e. typically within milliseconds. However, when the device is under bias, the funnel may be kept open by the constant flow of electrons/holes flowing from high to low potential energy.

While benign microlatch-ups may cause the circuit to malfunction until reset, the energy deposition is far to low to cause physical damages to the structure by Joule heating. Protection against such microlatch-ups therefore consist of detection of the failure followed by a power cycle of the device for a few ms after which nominal behavior is restored.

Conversely, will macorlatch-ups, where a power rail is shorted to ground, result in a massive increase of the current consumption. This power is deposited as joule heat in the region of the latchup, which may cause burn-out, melting or cracking of the affected region when the temperature reaches or surpasses the max allowable junction temperature. Protection against such destructive latch-ups are therefore based on an over current monitoring followed by an immediate power cycle, after which nominal operations is restored.

Naturally, all parts for the microASC has been selected for exhibiting very low latch-up sensitivity, wherefore latch-up events are extremely rare, even during operations in massive CMEs, typically les than 1 per 10years. However, latch-ups cannot be entirely eliminated since rare extremely energetic galactic particles may still trigger a latch-up.

The microASC latch-up protections is consequently designed to protect each microcircuit, in a way such that the maximum power rating is never exceeded. The microASC is therefore divided into protection monitoring blocks, grouping the parts such that if the nominal current increases more than 180% and less than the derated maximum current, the circuit is power cycled autonomously. This procedure result in that the worst case heating of any microcircuit, from a latch-up is limited to a few deg C. The correct operations of the latch-up protection has been verified in heavy ion accelerators.

3.9.6.2 SW/HW protection

The core processor is operated in full protected mode. This allows the different processes (procedures) to allocate their own part of memory in which they reside. Should a process try to access memory outside its own part (e.g. as response to an untrapped bitflip), a protection violation exception will be generated, and the microASC will be restarted. This mechanism provides a rigid protection against code and data corruptions from radiation induced bit-flips. As the protected mode structure ensures process and processing integrity, the full EDAC of all pipe-lines to/from the processor traps and corrects any Single Event Upset (SEU) that might have occurred in the runtime data and program memory or the data pipelines.

The combined effect from the above mechanisms renders an almost SEU-immune system, resulting in an extremely low setup frequency. Should a combination of faults enable a SEU to pass the filters, a high-level police program will trap all hung processes, resulting in a forced reset and a marginal loss of attitude update for 4.5 seconds. In LEO, the projected setup frequency is less than 1 per year.

3.10 Performance

3.10.1 Accuracy

The definition of the meaning of the term "star tracker attitude accuracy" largely depends on to which end the data is used. Typically, the accuracy is limited by noise sources that can be divided into three distinct classes by their frequency content.
Several noise sources are of a nature such that their impact on the attitude calculation is from update to update, e.g. photon-count noise, read-out noise, A/D noise etc. The RMS of all these noise sources (they are largely uncorrelated) gives rise to a noise in the attitude output also referred to as the Noise Equivalent Angle (NEA). NEA is the noise the user will experience with the camera pointing at approximately the same star field over time.

Because a well optimized tracker will be photon noise limited, the electro-optical pathway will have to be optimized for maximum throughput. This means that several components will exhibit deviation from a simple model, and thus when modelled give rise to calibration residuals. These residuals are typically of a nature such that they will vary with the star field observed, e.g. residual lens chromatic and geometric distortion, pixel to pixel variation, star-catalogue errors etc. Together with electronic noise in the second to minute range, these noise sources limit the accuracy further from the NEA value. The accuracy, including these terms, is referred to as the Relative Accuracy. The Relative Accuracy is the accuracy the user shall expect, when the tracker is operated within its envelope, including spacecraft

attitude motion. Again it is observed, that these noise sources are uncorrelated, and the total effect therefore shall be calculated via an RMS.

Finally, a set of slowly varying noises or biases exists. These changes over hours to years, and include effects such as gravity release, thermal stressing, radiation dose build up etc. These effects are so slowly varying, that they normally are perceived as biases, and consequently are added together. By adding the total effect of these terms to the RMS value of the relative accuracy, we arrive at the Absolute Accuracy, i.e. the accuracy with which the tracker, when inside its operational envelope, can deliver an attitude relative to the reference datum (J2000.0) at any time during the mission.

The microASC qualification process of all flight units includes a characterization of the NEA performance. The NEA can relatively easy be measured on ground, e.g. by mounting the camera on a mechanically stable platform. Through the sidereal rotation of the Earth the NEA can be measured for both meagre and rich star fields under the same platform conditions. Such measurements are mainly limited by the quality of the night sky, i.e. by seeing and local convection. Depending on the sky quality limitations, the real sky tests with the microASC typically deliver a cross axis NEA accuracy better than 1.9 arcseconds, with an accuracy around the boresight better than 19 arcseconds, both at galactic high and low attitudes.

Additionally, the NEA performance is assessed from a laboratory setup, using a calibrated artificial night-sky (OGSE). An example of the performance of the ASC PSD of such a characterization, measured for one of the GOCE flight units, is found in the figure below. It is noted that the PSD spectrum is flat up to the Nyquist frequency, i.e. the noise to be expected from the instrument is white. Typical values for the NEA accuracy are around 0.5 arcsecond cross axis and 5 arcseconds around the boresight.

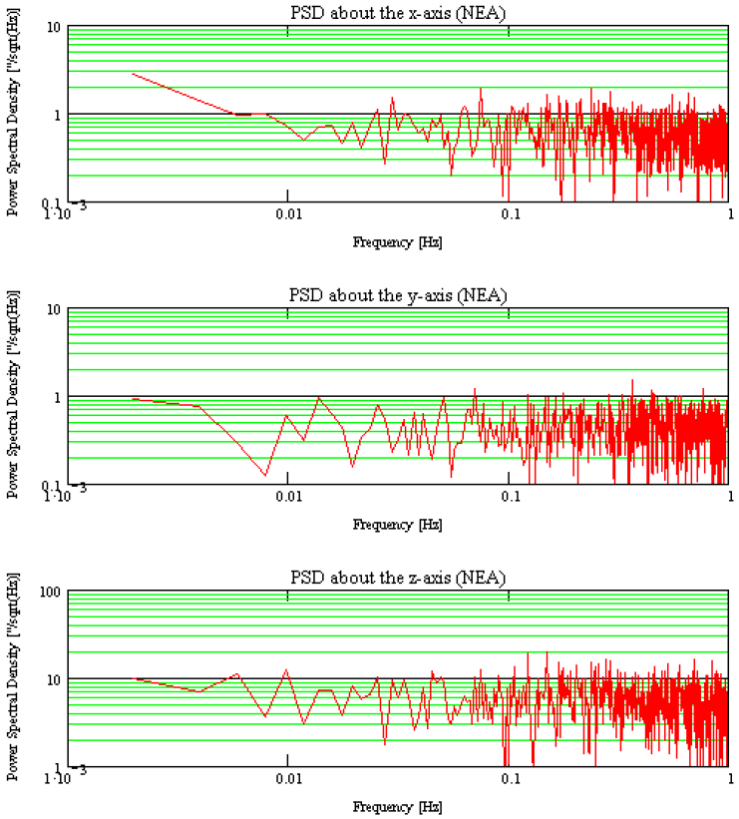

Figure 3: PSD plot for the NEA measurements for the three system axes. It is noted that the performance difference in the focal plane axes (x and y) is due to differences in the CCD geometry.

In-flight, only celestial pointing missions will view at a specific star field for extended times. For Earth observation satellites, the star field in the FOV will be constantly changing at a rate of some 100-300arcsecond/second. Therefore a good estimate of the NEA can be found by calculating the RMS of the attitude measurements from an orbit with the orbital mean motion subtracted. Using this method, the Ørsted tracker shows an NEA in the range of 1-2 arcsecond pointing and some 15-20 arcsecond around the boresight. Onboard CHAMP, which featured two sets of two cameras on a mechanically rigid structure, the orbital motion can be rigorously eliminated thus giving a high fidelity estimate of NEA. In this case, NEA values well below 0.5 arcsecond pointing are observed, and, just as important, the attitude noise, when comparing measurements obtained from the same pointing direction, but from consecutive orbits, i.e. 100min apart, shows a noise in the range of 1 arcsecond pointing.

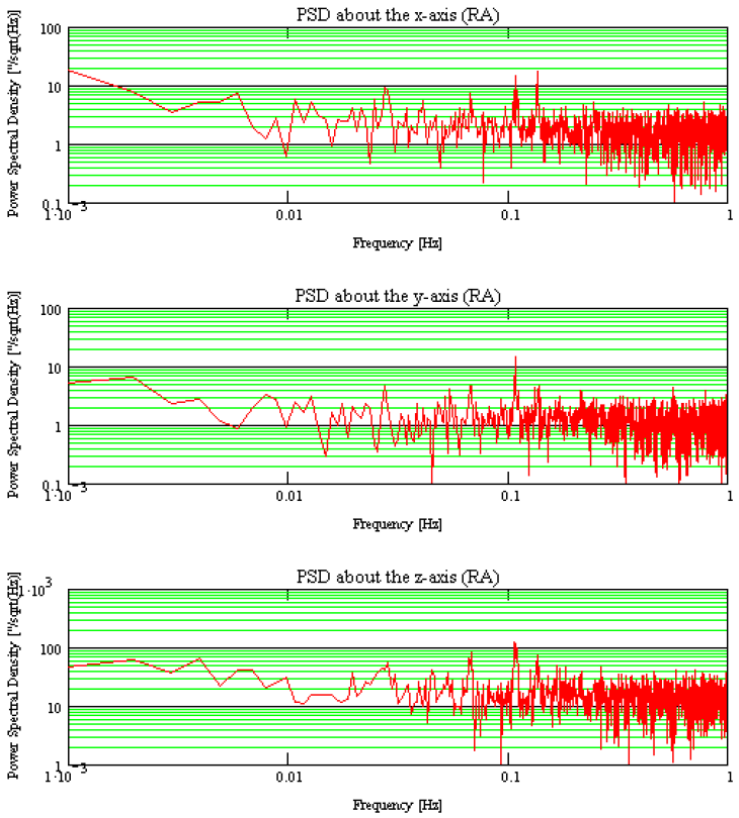

Figure 4: PSD plot for the RA measurements in the three system axes. The performance difference in the focal plane axes is noted again

In the case of CHAMP featuring a 20mm lens system, the ratio of the NEA pointing and the NEA about the boresight is 8.6 observed (8.0 theoretically).
On ground, the Relative Accuracy (RA) can be assessed, either by placing the camera on a stable platform, using the sidereal motion to generate the shifting star fields, or by mounting the camera on a telescope platform so as to perform a predefined attitude motion. The first method is limited by the air stability, and/or the available attitude motion, the second is limited by telescope motion jitter/inaccuracies. Using the stable platform, the microASC typically delivers an RA of 2.0 arcsecond pointing and 20 arcsecond around the boresight.

The microASC qualification process of all flight units includes a characterization of the RA performance. As an example of the ASC performance, the PSD of such a characterization measured for one of the GOCE flight units is found in the figure below. Again the PSD spectrum is found to be virtually flat, and the noise of the instrument to be white.

In-flight, the orbital motion and attitude control accuracy will influence the estimate based on measurements from a single camera. In the case of CHAMP the difference in the attitude measured by a set of cameras may be used to generate a better assessment, although this assessment may include substantial thermal biases. Using the latter method, typical values of RA of 2-2.5 arcseconds pointing are found.

The Absolute Accuracy (AA) is virtually impossible to verify experimentally on ground. This is because the required stability of the test platform exceeds what realistically can be achieved, and because the day to day, and seasonal variations in the atmospheric conditions will generate far larger biases than what is expected from the microASC. Therefore, the thermal and radiation dose buildup effects have to be found from analysis. In-flight, the spacecraft's thermal stability will typically be the limiting factor.

The microASC camera unit is mechanically made from isotropic titanium, mounted to the spacecraft structure via a kinematic mount. Assuming that the thermal gradient from CCD to the mounting flange is less than 3.5C, which is the typical in-flight value, the maximum thermal bias is less than 1 arcsecond. The radiation induced bias has been estimated from accelerator irradiated CCD's to be less than 2 arcseconds (EOL).

3.10.2 Robustness

The microASC S/W has been developed with very strict requirements to robustness. That is, the microASC is able to perform in most situations and under all possible external effects. This section covers a subset of such situations.

3.10.2.1 Recovery from Blinding

The microASC is able to recover from sun blinding to full performance in a few seconds. This is achieved by a highly optimized control loop of the Automatic Gain Control (AGC) of the video data.

3.10.2.2 Radiation Damages and EOL Performance

The microASC gives full performance after full lifetime radiation dose. This is achieved by software handling of all radiation damages (hotspots and darkspots).
The EOL performance is insured by measuring the microASC performance during continuous injection of artificial hotspots into the source images, corresponding to the EOL radiation dose.

3.10.2.3 Non-stellar Objects

The microASC gives full performance, when non-stellar objects are present in the FOV. Examples of NSO's are: planets, comets, space debris, or other satellites. Centroids from such NSO's are rejected in the software and not used in the attitude determination leading to bias free measurements.

3.10.3 Timeliness

3.10.3.1 Initial Acquisition

The microASC is able to deliver a 3 axes attitude determination from no a priori knowledge of the attitude (Lost-in-Space function). The time duration for deriving a Lost in Space attitude solution is approx. 80 ms after the image is available to the star tracker algorithms.

3.10.3.2 Tracking

When the initial acquisitions have been established for each of the CHUs the instrument enters tracking. In this functionality it builds up dynamics knowledge of each CHU, both it is inertial motion components but also relative orientation to the other attached CHUs.

Using these models, the attitude is extrapolated with high accuracy seeding both centroiding and pattern matching algorithms. This leads to an extremely robust operation, but more importantly, it can be handled with a very low latency. During nominal tracking operation, an attitude solution is typically derived within 20ms after the image is available to the star tracker algorithms.

3.10.3.3 Attitude Data Availability

Data availability from a star tracker is essentially limited by four factors, which affect the basic operation adversely. These are: Bright objects, radiation, slew rate, and jerks/shocks. The most important of these is the blinding. For Earth orbiting missions, the dominant sources of blinding are the Sun, the Moon, and the Earth. Normally the mission design precludes the tracker from viewing the Earth, but for most missions both the Sun and the Moon will get into the FOV at times. Two phenomena play a role in the blinding process; even though the luminous object is quite small, and ideally should only affect a small part of the detector viewing area, the luminosity is high, and both the secondary point spread function of the optics and an overload phenomena in the detector called blooming come into play.

In the case of full Moon blinding, the blooming will adversely affect the entire range of columns having pixels directly hit by the moonlight. Furthermore, the secondary point spread function of the optics will generate an area around the directly illuminated pixels that will see increased background levels.

In the case of the microASC, the lens is especially designed to handle large bright objects as the Moon. Hence, proper operations, with only slight to negligible effects, are seen with the Moon in the FOV in most cases. Only when the Moon is full (phase>75%), and the Moon is in the central third of the FOV, tracking is lost.
The sunlight is so powerful, that scattered stray light will prohibit proper operation, even when the Sun is some angle out of the FOV. For this reason trackers are fitted with stray light suppression baffles.

The effect responsible for this is again the secondary and tertiary point spread function, which, coupled with the diffuse or reflected stray light, give rise to an (highly) increased background level of the detector image. At higher levels of stray light, the detector then produces an image of the stars superimposed on this background resulting in a vanishing signal to noise ratio. Therefore, the first effect of this kind of stray light is to generate attitudes of lesser accuracy, and then, when the detector pixels reach their full well capacity, or the offset controls of the tracker saturate, the tracking ceases to operate.
In the case of the microASC, operations close to the Sun are made possible by means of a two stage baffle system, combined with a large offset-span regulation. The user can then choose to let the microASC operate closer to the Sun, accepting lesser accuracy, or to let the microASC stop operations, when the stray light becomes excessive, thus ensuring high quality data at all times.

A special problem occurs in the transition phase between nominal illumination levels and solar blinding. In this phase, the sunlight, reflected off the internal parts of the baffle and into the lens system, will generate a complex pattern of background illumination on the detector. If the tracker is required to try to generate attitude updates under these conditions, the process time may increase so much, that attitude updates have to be skipped, if data timeliness has to be maintained. On the CHAMP mission, this phenomenon is responsible for a loss of some 0.5% of the updates at times, where one of the cameras are grazing or going through the Sun.

Stray light analysis is obtained in terms of a simulation tool. This tool has been verified against in-flight measurements, wherefore stray light tests are not performed.
Ionizing radiation, in the form of energetic particles, will have an impact on the data availability, when the flux-rate comes over a certain level. This is because particles passing the detector deposit charges (e.g. up to 2000e-/p+) will be detected by the tracker. The

tracker will then have to spend part of its processing on detecting and removing these charges, and, worse, when the flux becomes sufficiently high, inevitably some of the particles will hit close to the centroid of a real star, thus generating an offset of the centroid.
The microASC handles the first effect by means of a fast morphological filter that can handle several thousand particles per image. The shift in the centroid can only partly be removed, so even though it is efficiently offset by using a high number of stars for the tracking, it will give rise to higher noise levels at times with a high particle flux. E.g. the CHAMP trackers gave attitudes with a noise in the range of 10-15 arcsecond during the two major solar storms of 2000.

3.10.4 Quality of Attitude Data

The microASC provides a *validity* flag, a *BBO* and a *quality index* within each attitude message.

- The *validity* flag indicates, if the derived attitude quaternion is valid.
- The *quality index* indicates the fitting of the measured positions of the stars used for attitude determination versus catalogued positions of these stars.
- The BBO flag indicates that a *Big Bright Object* was identified in the source image. The brightness of these objects are so strong that the image background is no longer even, which will lead to a bias in the derived centroids.

Dependent on the on-board attitude accuracy requirement, the quality index and the BBO flag can be used to weight the solution for the on-board AOCS filtering.

3.10.5 Date of attitude data

All the attitude packets are time stamped. The datation corresponds to the time of the center point of the integration (COI) phase and it can be expressed in the microASC own clock, the OBC reference time or the GPS time depending on the Customer timing philosophy. In addition, the image integration is synchronized to a PPS pulse, such that a constant phase between PPS and COI is achieved. The timestamp jitter is less than 10µs.

3.10.6 Update rate

The update rate of the microASC is coupled to the image integration period, such that a 100% duty cycle of the stellar light irradiation is obtained. This integration time (T_{int}) can be set to eight different periods, ranging from 1/8s to 16s. For optimal performance, integration periods of either 0.25s, 0.5s or 1s are recommended. A longer integration period will result in a higher accuracy, whereas a shorter integration period will result in shorter data latency.
The update rate defined as images processed pr. second can be determined from the integration period and the number of attached CHUs ($N_{CHU)}$ using the following formulae:

Update rate = N_{CHU}/T_{int}

The microASC can support a maximum of 4 CHUs. E.g. a configuration of 3 CHUs operated at T_{int} =0.25s will result in an update rate of 12 solutions/s.

3.10.7 Exclusion angles

The exclusion angles of the microASC is defined as the angles between the electro-optical axis and the Sun and the Earth respectively, where attitude determination is impossible due

to CCD saturation. The exclusion angle is directly a function of the available volume, i.e. the longer the baffle the smaller the exclusion angle. At any given baffle length and volume, a design for a minimum exclusion angle has to be made.

The microASC baffles are always designed as so called two stage baffles, that is, an inner stage grazing the FOV, and an outer stage intended to suppress the sunlight incident on the inner stage. This design gives a better exclusion angle than what can be achieved using a single stage baffle, however, the immunity towards dust contamination and mechanical misalignment are much higher in a two stage baffle system when compared to a one stage system of the same size.
The microASC baffle system performance is verified in the laboratory by means of multi-order backwards scatter simulation. The simulator has been verified by comparison with in-flight performance.
No exclusion angle is specified for the moon because the effects of the moon in the FOV are limited to:

- Loss of accuracy;
- Possible loss of data only if the Moon is within the central 7 deg. (full angle) of the FOV.

3.10.8 Multi Head Operations

The microASC features the possibility of connecting 1 to 4 CHUs to the microDPU. The connected CHUs can all be operated in parallel and will provide individual attitude solutions. With the double DPU the CHUs may be assigned to either of the two fully redundant Data Processing Units. The assignment of the individual CHU is configurable and can be changed in-flight by telecommand.
If the CHUs are controlled from the same DPU, the image integration will be synchronized, resulting in individual attitude solutions timestamped at the same point in time (center of integration).
The option to use multiple camera heads has the following key characteristics:

- Reduction or removal of S/C attitude keep-out zones (e.g. blindings)
- Accuracy improvement
- Platform thermo-mechanical characterization

Reduction or removal of S/C attitude keep-out zones: Any optical system will be susceptible to blinding from bright sources or obstruction of the FOV. For the microASC the major obstruction sources are blindings from the Sun and the bright Earth and obstruction from the dark Earth. By using multiple Camera Head Units continuous operations (valid attitude solutions) can be ensured, if at least one CHU remains un-blinded/un-obstructed. The capability to cope with blinding of individual CHUs can greatly improve the S/C agility and reduce attitude profile constraints. Furthermore, the requirement for the exclusion angle performance of the baffle system can be reduced, hereby reducing the volume needed for the straylight suppression baffle. The table below gives an example summary of the characteristics of multiple heads.

Accuracy improvement: The attitude solution of the individual CHU is by geometry an-isotropic. The pointing direction of the CHU boresight has the best accuracy, while the roll about boresight is approximately 8-10 times less accurate. Since the attitude solutions from multiple CHUs will be timestamped to the same point in time (center of integration), the

attitudes from the individual CHUs can be combined to obtain an improved estimate of the SC attitude. The major improvement comes from the combination of CHUs with approximately orthogonal boresights. If several CHUs are collocated on a highly stable structure (e.g. optical bench) high attitude accuracy (better than the boresight pointing) can be achieved in all three degrees of freedom.

Platform thermo-mechanical characterization: The platform structure carrying the CHUs will typically have thermo-mechanical variations in the range detectable by the star trackers. Hereby the stability of the platform can be estimated, and if sufficient information is available variations may be modelled. The structure characterized in this way includes the following examples:

- A sub system measurement platform, e.g. telescope
- The entire SC structure
- SC appendages, e.g. booms carrying instrumentation

Number of CHUs	Optimal inter boresight angle	Boresight configuration (from zenith)	High accuracy 3D attitude (% of time)	Optical bench stability measurement (% of time)	Optimal CHU / baffle size (LxWxH) mm^3
2	~90°	2 x 45°	95%	95% reduced accuracy	300 x 170 x 150
3	~3 x 90°	2 x 45°	100%	95% full accuracy 100% reduced accuracy	400 x 130 x 115
4	~4 x 90°	2 x 45°	100%	100% full accuracy	400 x 130 x 115

Table: Example characteristics of multiple CHUs for a Low Earth Orbit, 3 axis stabilized, non-sun synchronous S/C.

3.10.9 Satellite Motion

By noting that a star tracker is photon noise limited, it is evident, that the accuracy is a function of the square root of the integration time. If the integration time is doubled, the accuracy is approximately doubled.

When the star field is moving across the FOV, the photons from the star is smeared over more pixels. This effectively results in a decreased signal to noise ratio. Higher attitude motion will therefore result in a decreased accuracy. When the rate is further increased, the smearing effect will be so large, that the fainter stars will drop below the detection threshold, thus increasing the noise further. At very high rates, a substantial amount of brighter stars will be lost, because they move outside the FOV during the integration time, thus efficiently decreasing the FOV of the tracker, and thus limiting the accuracy further.

The slew rate performance is assessable on ground, by mounting the CHUs on a telescope drive to generate controlled, known slewing rates.

Generally S/C rotation can be transformed into two different components of rotation as seen by the microASC: Cross boresight, and about boresight rates. The cross boresight rate is the most critical. The microASC theoretical values of performance versus rates are listed below.

Integration time [sec]	Max rate (Cross) [deg /sec]	Max rate (around) [deg /sec]	NEA(1Φ) [arcsec]
1	1	8	0.4
0.5	2	16	0.8
0.25	4	30	1.8

At the above rates the probabilities of valid attitude measurements are > 99%. It is important to note that the above rates are difficult to substantiate via ground tests on real-sky, partly because of the unavoidable drive noise of the test platform, partly because that the higher rates conflict with dome slit sizes and test time, and partly because of an unusual high requirement to the atmospheric stability and clarity over virtually the entire night sky. Hence validation is typically only performed at selected rates.

	Max measured Sweep Rate [deg/s]	Max Measured Acceleration [deg/s*s]	Max Measured d(Acc)/dt [deg/s*s*s]
RA	4.2	5.3	10.8
Dec	4.1	4.4	4.6

The values listed above are typical examples from a real-sky test, with the CHU's mounted on an astronomical telescope. The telescope then functions as a precision drive for generating the desired test rate conditions. As seen from the above test example, both the acceleration as well as the jerk levels are quite high during the tests despite a telescope above 1 ton.

It is also important to note that the microASC operates properly well above the listed rates. E.g. a 25% valid update rate was measured at 41 deg /sec around boresight rate.

3.10.9.1 Higher Slew Rates

High slew rates have three impacts on the data availability. Firstly, the signal to noise ratio is decreased, and secondly, the effective FOV of the system is decreased due to stars straddling the FOV border, thirdly the centroiding function will have to cope with more complex star centroids as the motion rates increases.

The increased noise level will have the impact, that the tracker might take more than one update to fix from lost in space, because the data quality of any single image may be too poor to allow for a robust solution of the lost in space problem. This effect is negligible at rates below 0.6 deg/sec, but becomes dominant at rates above 4 deg/sec, disregarded what integration time is used.

The decrease in effective FOV is proportional to the slew rate and inversely proportional to the integration time. Therefore, a short integration time shall be used, if higher attitude data rates are to be supported.

The combination of the above effects is minimized by choosing a short integration time.

3.10.9.2 Performance on Spin Stabilized Satellites

The high tolerance to satellite motion is not just an enabling technology for agile satellites, but can further be used to enable high accuracy star tracking on spin stabilized satellites. The microASC is already flying on several such missions, and flight heritage has been gained with spin rates of 1, 2 and 4RPM.

In order to be tolerant to the high spin rates, the CHUs shall be mounted such that they point relatively close to the spin axis. The higher the spin rate, the closer to the spin axis the CHU shall point (the smaller cant angle). Example heritage configurations are given in the table below:

Spin Rate [RPM]	Spin Rate [°/s]	Cant Angle [°]
1	6	13
2	12	13
3	18	10
4	24	6.5

3.10.9.3 Optional Spin Pulse Interface

On spinning satellites, an onboard measurement cycle will often be synchronous to the spin phase. This spin phase is traditionally derived from sun sensors, followed by integration of inertial sensors.

Enabling star trackers on spinning platforms offer a much higher accuracy on the derived spin phase; partly due to the intrinsic higher accuracy of star trackers; partly by eliminating divergence problems from the inertial sensors. In case of less performing onboard computers, the microASC offers optionally to output a pulse on a dedicated digital output line, each time the satellite spin reaches a certain phase. Two possibilities for controlling the phase exists:

- *Sun locked*. The microASC mimics a sun sensor, e.g. as backup during eclipse periods. Each time a certain vector in one of the CHUs reference frames passes the sun meridian, the pulse is output. The instrument needs the absolute time for deriving the sun vector (assuming an Earth orbit)
- *Inertial locked*. Each time a certain vector in one of the CHUs reference frames passes a certain vector in the inertial coordinate reference frame (ICRF) meridian, the pulse is output. No additional input is needed

Both CHU reference frame vector and ICRF vector are given as system parameters and can be trimmed in flight.

3.10.10 Missing stars

The internal structure of stars causes temporal fluctuations of their luminous output. This fluctuation causes the apparent magnitude of most stars to vary. Several stars fluctuate several levels of magnitude over the course of weeks. It is therefore important, that all autonomous star trackers do not rely on exact star magnitudes, and, that the tracker is tolerant towards missing stars, so as to be able to acquire and update on star fields, where several stars temporary happens to be below the star trackers threshold. Obviously, this tolerance also guarantees that the tracker can still operate, even though the star catalogue is incomplete.
The microASC SW is designed such that robust acquisition is maintained, even if up to 70% of the stars are missing. The tracking can be maintained if only 20% of the expected stars from the catalogue are available in the FOV.

3.10.11 False objects

Most star trackers do have a lower star intensity limit between mv5-mv7. This means that a few non-stellar objects must be expected in each frame. These objects are typically galaxies, other spacecrafts, planets, comets, or asteroids. A star tracker must therefore be capable of maintaining proper operations with several non-stellar objects in the FOV.
Furthermore, ionized particles passing through the detector will give rise to charge depositions that often has a spatial distribution similar to that of a star centroid. Therefore, the star tracker must be able to handle a substantial number of objects at times with increased particle levels, e.g. during a solar storm or while operating in the South Atlantic Anomaly.
The microASC is designed to deliver robust and accurate tracking with several tens of non stellar objects in the FOV. In-flight data from the ASC show, that an average of 3 non-stellar objects are detected per frame, and that these objects always have been correctly detected and suppressed. Furthermore, during severe solar activity, the microASC in-flight data show, that it is capable of handling radiation induced spots at levels up to 100.000 times the average quiet time level, this means that more than 2.000 false objects per frame have been correctly detected and discarded.

3.11 microDPU Processing Power

The design of the microDPU enables the simultaneous operation of up to four CHUs. The load of the DPU CPU depends on both the number of CHUs in operation and the update rate. Further, non-nominal operations may contribute to an increased DPU load, for example. an increase of the number of hot spots during a solar storm.

Figure 6 shows the nominal case the load of the DPU as a function of the number of operated CHUs and the ***true*** update rate per CHU. For all the configurations contained in the figure, plenty of margins to the maximum load of the DPU is present. Thus the sustaining of the CHUs even during non-nominal conditions is generally ensured.

In case of the redundant double DPU, the figure applies to each of the sides of the DPU.

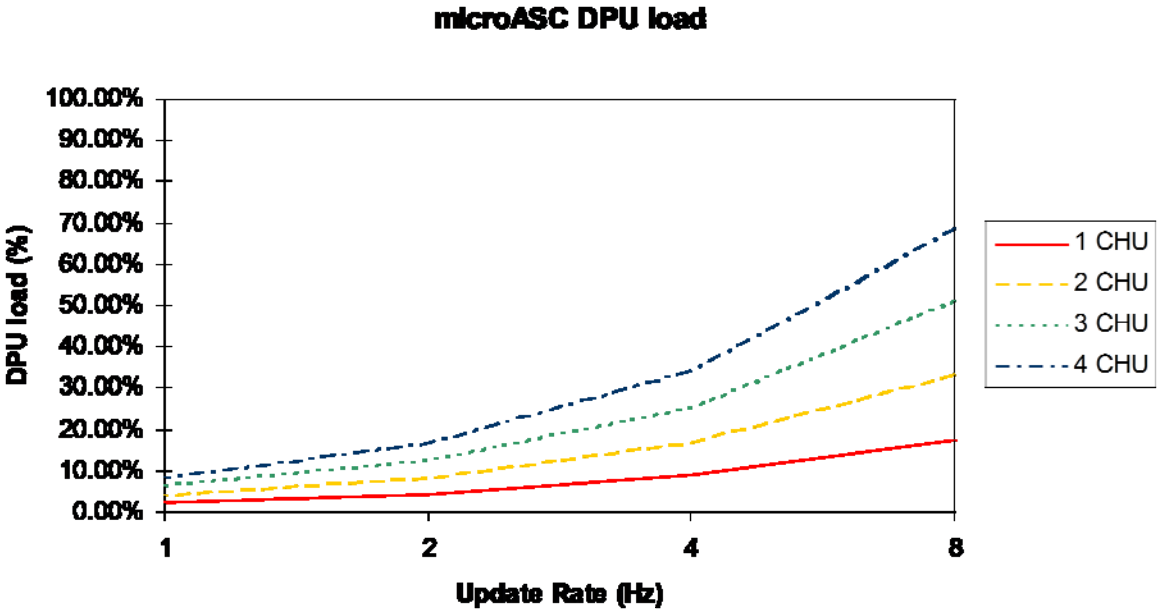

Figure 5: The microASC DPU performance as a function of the true update rate per CHU and the number of CHUs operated by the DPU

3.12 Post Delivery Support

Due to the possibility of unexpected events during a spacecraft launch, DTU offers to support the first part of the Launch and Early Orbit Phase (LEOP). During the LEOP it is recommended to verify the performance of the instrument by an optical parameter and sensitivity optimization:

Due to mechanical tolerances in the optical systems and in the CHU assembly, minute differences in the optical characteristics and sensitivity between the delivered flight units will be present. The CHUs are therefore individually characterized on-ground. It is our experience that performing such a characterization in the natural environment of the instrument, i.e. using real-sky tests, improves a laboratory pre-characterization by an order of magnitude. However, even the on-ground real-sky test suffers from drawbacks. Bringing the instrument to an astronomical site will reduce the air pressure by about 40% (depending on site altitude), but the remaining 60% air-mass will generate an optical aberration. This

aberration stems both from changes in refraction index in the medium between the lens elements, but also due to very local atmospheric conditions also referred to as "seeing". A good understanding of these effects has been established from previous programs, which are taken into consideration during the characterization phase.

The microASC offers the possibility to propagate the images acquired by the CHUs via telemetry. Based on five to ten of such images, a complete re-characterization of the optical and sensitivity parameters can be performed, which either will lead to a confirmation or to a proposal for updating the parameters.

DTU usually offers to partake in such a task as part of the LEOP support.

4 Design Aspects

Throughout the design of the HW, the emphasis has been put on accuracy, functionality, low power, low thermal stressing, mass, and size. Throughout the design, SMD technology has been utilized, increasing the board density and maximizing the mechanical stability. This has led to a compact design with a very low IC-count, full inline EDAC, and a very high data handling capacity. In several cases commercial chips were proven to be by far the best, and in some cases even the only choice, e.g. the CCD-chip.

Due to this design procedure, all chips used in the design have been thoroughly screened for radiation tolerance with respect to total-dose, dose-rate for Single Event Upset (SEU), and Single Event Latch-up (SEL). After the acceptance screening, a number of chips from the same batch are acquired, and the tests are then performed again on samples from each batch in order to confirm the validity of the screen-tests for that batch.

This selection process ensures correct operation during exposure to solar wind and trapped protons (Van Allen belts). To cope with SELs generated by the rare cosmic particles, each circuit block is protected by individual latch-up protection circuitry.

Thermally, the design has been verified to conform to the goal, so as no component has a temperature that deviates more than 9EC from the box surface in vacuum. The low thermal gradient, which is associated with the low power dissipation and strong thermal coupling, results in an extraordinary thermal cycling resilience and provides for a very high reliability figure, as proven by the accelerated lifetime test.

The thermal analysis is accomplished by a thermal model, characterizing the thermal loads of, in particular, the camera head. The verification of the thermal model is based on data collected from in-flight measurements.

The compact design and the miniaturization provide for a rugged unit with low amplification factors and high resonant frequencies, resulting in high shock and vibration level tolerances. After assembly, the circuitry is tested for function and parametric variations, upon which a burn-in procedure is performed. Accelerated life tests are performed on sample boards from the batch.

Throughout the design, emphasis has been put on making system performance independent of the degradation of various parameters with age or radiation doses. E.g. the autonomous offset and gain control in the analog signal path from the camera is able to cope with large variations in the CCD-chip sensitivity, the Correlated Double Sampler sensitivity, or the line amplification. Other examples are the SW-maintained hot-spot database that handles radiation induced (temporary or static) defects in the CCD, full utilization of the inherent HW protection mechanisms in the processor used to trap SEU's, and full in-flight upload capability of the SW except from a small core loader.

5 Vision Based Sensor

The microASC includes additional modes of operation which extends the normal attitude determination system. Such extended feature is the Vision Based Sensor (VBS) system, which provides the microASC with the functionalities of Non-Stellar Object Tracking, and as a Rendezvous- and Docking Navigation sensor.

5.1 VBS Modes of Operation

The VBS system has two main modes of operation, where the hardware of the CHUs present in the microASC system determine their availability. These main modes includes; Far Range mode which can provide Line-of-Sight (LoS) VBS solutions and is available using standard star tracker CHUs, and Short Range mode which can provide 6-Degrees-of-Freedom (6DoF) solutions of a target spacecraft flying in close proximity and requires minor modifications to the standard lens system on a dedicated VBS CHU.

Furthermore, the VBS system can consist of a number of cooperative hardware elements, supporting the cameras with mire points and high-precision references. These elements enable determination of pose and position with high reliability and in scenarios where structure based images are insufficient.

The modes of operation for the VBS are controlled by defining the CHU configuration in the system parameters of the microASC, and can be modified in-flight. Dependent on the hardware, the CHUs are configured either as a Far Range CHU providing Far- or Intermediate Range solution, or as a Short Range CHU providing Intermediate- or Short Range solution.

The nominal range of the VBS system spans from the detection limit of a standard CHU (~M_V 7) down to the minimum distance of a Short Range CHU (~40cm). For overlapping in between the two CHU configurations, an Intermediate Range solution is possible for both. In Figure 6, is illustrated the overlapping and comparable accuracy for the different VBS solution methods is illustrated.

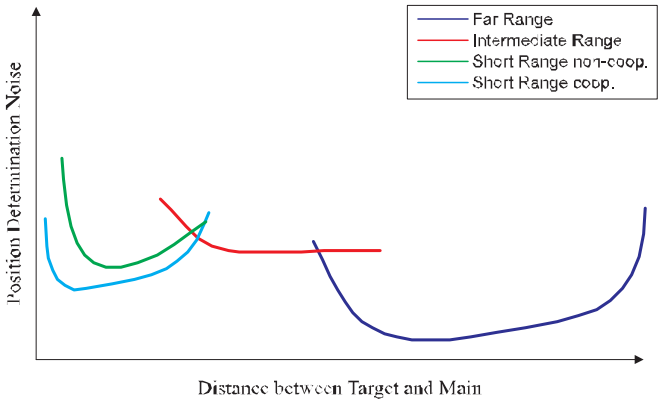

Figure 6: Cursory illustration of VBS mode overlapping.

The VBS solutions and their sub-modes are defined as:

- **Far Range:** Stars can be detected in coordination with detection of the Target spacecraft, enabling attitude determination of the Far Range CHU. Solution is given as inertial line-of-sight.
- **Intermediate Range:** Stars are undetectable due to the brightness of the Target spacecraft, and no features of the Target can be detected. Solution is given as either inertial or relative line-of-sight.
- **Short Range:** Features of the Target spacecraft are detectable. Solution is given as relative 6-degrees-of-freedom.
  - **Non-cooperative:** Target spacecraft is passive, only illuminated by the ambient scene radiance.
  - **Cooperative:** Target provides detectable feature points in specific geometric patterns.

5.2 VBS Accuracy

The accuracy for the VBS system differs dependent on the CHU configuration and the solution availability.

For the Far Range CHU providing Far Range solutions, the accuracy of the line-of-sight pointing corresponds to the accuracy of which the microASC system can perform centroiding. Inflight experience from the PRISMA mission has shown a RMS noise <10” at a distance of ~3km between Main and Target spacecraft.

For the Short Range CHU providing Cooperative Short Range solutions, the inflight experience has shown that the accuracy can be approximated by the scale law with the following parameters:

Lateral position accuracy:	[dx, dy]	= 0.5µm * z_0/f
Distance position accuracy:	[dz]	= 0.5µm * $z_0^2/(w_0*f)$
Pitch, yaw accuracy:	[dx’, dy’]	= atan(dz/w_0)
Roll accuracy:	[dz’]	= atan(dx/w_0)

where,

z_0 is the distance to the Target spacecraft.
w_0 is the width of the Target spacecraft.
f is the focal length of the Short Range CHU.

Ex: with z_0 = 2m, w_0 = 0.6m, f =20mm =>
[dx,dy,dz] = [50µm, 50µm, 180µm] and [dx’,dy’,dz’] = [60”, 60”, 20”]

6 The MIRU Augmentation

The Micro Inertial Reference Unit (MIRU) constitutes an optional functional augmentation of the standard microASC configuration, which is co-integrated with the standard microASC camera head unit (CHU). Utilizing a novel arrangement of five separate MEMS-based (micro-electro-mechanical systems) inertial sensors for a total of 11 sensitive axes, the MIRU realizes a high bandwidth 6DOF sensor system. The full inertial sensor complement consists of 4 dual axis linear accelerometers and a single three axis rate gyroscope.

The MIRU integrates seamlessly within the existing functional envelope of the microASC instrument without affecting nominal startracker operations. All data generated by the MIRU are transferred to the user through existing interfaces, and as the MIRU hardware integrates fully into the titanium backhousing of the CHU, the augmented CHU retains all native mechanical and electrical interfaces. The only appreciable, physical impact is an 8mm increase in the depth of the CHU backhousing in addition to a ~100mW increase in the CHU power consumption. Similarly, the native performance characteristics of the microASC remain completely unchanged as does the radiation tolerance levels.

The MIRU sensor suite has been designed to harness the complementary nature of optical and inertial sensors while providing high availability attitude solutions over a wide bandwidth from DC to 200Hz. This co-integrated and intercalibrated combination of the microASC startracker and the MIRU augmentation uniquely presents the spacecraft designer with the option of designing a mission based upon one attitude sensor only.

6.1 Principles of Operation

Linear Motion Recovery:
The MIRU is capable of recovering relative 3DOF linear motion using double integration of the accelerometer outputs. Although linear motion recovery is not critical to most 3-axis stabilized spacecraft, this type of information is extremely valuable in close formation flying, rendezvous, and docking mission scenarios. Moreover, the accelerometers provide a means of assessing the quality of the onboard zero-g environment, mapping the nature of disturbance torques, monitoring physical deterioration of onboard movable joints, thruster performance characterization etc.

Angular Motion Recovery:
The MIRU sensor configuration is capable of recovering angular motion by two separate means, namely:

1. Direct integration of low bandwidth gyroscope angular rate measurements.
2. Double integration of differentially coupled high bandwidth linear accelerometer measurements.

This dualistic approach to angular motion recovery allows the MIRU to cover a much larger operational bandwidth than conventional IMU designs, whilst taking full advantage of the absolute integration error bounding with arcsecond level accuracy offered by the microASC star tracker updates.
The first method utilizes the angular rate measurements provided by the MEMS gyroscope and estimates angular motion through single integration of the data. Acquired over a fairly low bandwidth, these measurements provide the user with a continuous stream of angular rate data and angular motion estimates that may be used to bridge microASC attitude

solution outages during CHU blindings or when subjected to high angular rates by the carrier spacecraft.
The second method utilizes the differential coupling of the dual axis accelerometer pairs in the MIRU sensor complement to estimate angular motion. Arriving at the estimated linear displacement pertaining to each accelerometer through double integration, the angular displacement for a given sensor baseline L may be tabulated as illustrated by the following figure.

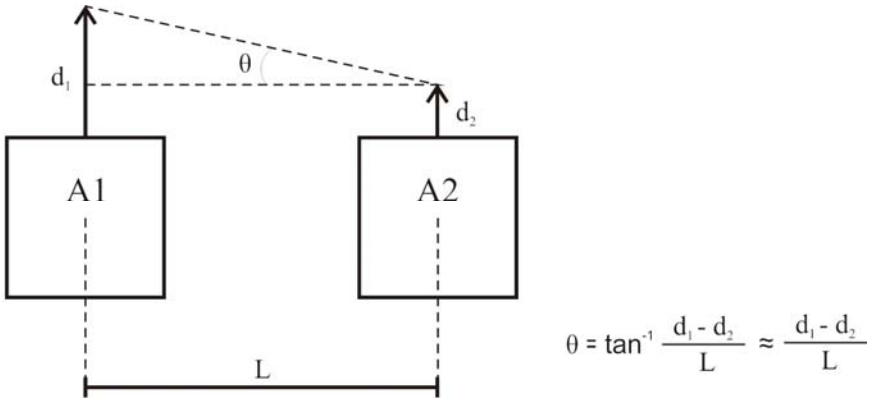

Figure 7: Determining angular displacement from differentially coupled linear accelerometers

Utilizing this principle provides unique access to high bandwidth information about platform attitude jitter and dynamics, far beyond those accessible by traditional attitude determination instrumentation suites.
Inherently, the double integration entails higher error accumulation rates than those incurred by a gyroscope based solution. Yet, on timescales of the microASC standard update rate and below, the accumulated error remains on par with that of many fiber optic gyroscopes, but with a much higher operational bandwidth.

7 Autonomous On-Board Orbit Determination

Another unique feature of the microASC is its capability to determine the position and the orbit of the spacecraft without any a priori knowledge.

This capability is of particular interest to any spacecraft flying above the GPS satellites and into deep space for several reasons:

- To autonomously and automatically re-point the on-board antennas to ground in case of a broken link;
- To increase the robustness, the flexibility, and the science return;
- To allow true closed loop operations and control;
- To reduce considerably operational constraints and costs.

The first point is of special relevance even for the missions that will fly using the traditional ground-based navigation.
Some missions have been lost, because it was not possible to re-establish contact with the spacecraft after loss. In some cases, such as the Russian missions to Mars, where the contact was lost because of a wrong attitude maneuver, the mission could have been recovered if the on-board systems were more autonomous.

Indeed, the robustness of the mission against mishaps mainly relies on preventing hazardous situations. This is achieved by constraining the system design, the trajectory planning and the attitude maneuver. In fact, in case of loss of contact, the ground stations are powerless with regards to re-gaining control of the vehicle to re-establish the communications. Normally the spacecraft can only set itself in the safe configuration with no capability to actively seek the earth.
However, knowing the ephemerides of the earth and determining its position, the spacecraft is able to autonomously point the antenna toward earth to re-establish the contact.
It is also important to stress that this capability is completely general (not tailored to any specific project/orbit), completely autonomous and it does not require any, even approximate, a-priori knowledge, i.e. it solves the lost-in-space problem.
The position, the velocity, and the orbit are determined by the observation of the apparent angular position of the planets w.r.t the background stars. This function only requires an accurate knowledge of the mission elapsed time.

The microASC AutoNav function is an added-on faculty. It runs on the instrument used to determine the attitude without any loss of performance, and it can be switched on/off by simple command. It does not require any dedicated instrument.

8 Support to Other Instruments

The microASC has been designed to integrate and to support other instruments.
With a minor penalty in terms of mass and power, extra decks can be added to the microASC, which provides them with the power and the TM/TC capabilities.
In this way magnetometers and accelerometers can easily be assembled in a miniaturized highly efficient unit.

9 Ground Support Equipment

9.1 Overview

The microASC comes along with a suite of support equipment to be used at different stages in order to be able to verify reliably and determine the instrument's health at any time, support the design of the AOCS from the earliest stage, ease the integration of the microASC into the spacecraft system (space and ground segments) and to learn simply how to operate the star tracker.

9.2 SimAsc

The SimAsc program is a piece of C-code that simulates the behaviour of the Advanced Stellar Compass. The program simulates the behaviour of the microASC and can be interfaced with CAD tools, e.g. Matlab and SW system simulators.
The program simulates several effects, such as time delays (offset, exit, process), noise contributions (NEA, residuals), and the attitude dropouts (process timeout, sun blinding).
The use of the SimAsc shall be envisaged only at the very early stage of the development, or when HW in the loop is not possible.

9.3 Simulation Mode

To simulate the microASC performance while maintaining a high degree of fidelity in the system, the use of a special feature of the microASC SW, already developed and extensively tested, is advantageous to verify the flight HW. This is called the *simulation mode*. In simulation mode, SW generates an image of the sky visible to the CHU, using the star catalogue. This map is then corrupted by adding false objects, by deleting and misplacing stars, and by adding noise and other effects. Finally the map is superimposed to images taken by the camera with the cap on to add the camera response characteristics. The images generated are fed into the microASC SW.

There are three different simulation modes providing the possibility of testing various dynamical conditions:

1. Full user control: The attitude and apparent drift are directly controlled via the test-computer that uploads a new attitude. This mode is intended for verifying complex maneuvers, and for checking the real-timeliness, and the attitude flags.
2. Pointing user-control: The pointing direction and a drift rate are uploaded to the microASC. When the next image is ready for processing, an attitude simulation process, as described above, will take place. This simulation will proceed until a new simulation command is issued. This mode is intended to verify AOCS actuator signal sign and size.
3. Relative user-control: The microASC is seeded with the desired pointing direction and rates of change values. It will then automatically use the latest calculated value of the attitude to seed the next simulation step. This mode is intended for closed loop simulations, simulating real attitude manoeuvres and control.

To improve the system performance in open loop tests, the microASC can use previously downloaded images with known attitudes during the tests.

To support the closed loop simulations and tests in a testbed, the images shall be generated in real-time using the S/C attitude quaternion and rate computed by a dynamics simulator. This solution is very close to what could be defined as *ideal*.

9.4 Optical Stimulator (OGSE)

The Optical Ground Support Equipment (OGSE) is a device designed to test the quality and the end to end performance of the CHU, after the CHU is integrated in the spacecraft and real-sky tests are no longer possible. It allows polarity checks, attitude measurements, image quality assessment, and end-to-end tests of the microASC.

The OGSE specifically consists of a hardware Star Field Stimulator (SFS) together with a subset of features of the highly versatile EGSE (see below). The stimulator produces a number of synthetic star triplets to resemble a synthetic star field. The stimulator itself mounts either directly on the CHU or on the baffle system, depending on the chosen design. It is operated manually and is designed to be easy to handle.

All materials of the stimulator are selected, such that they allow for operations under extreme conditions, e.g. in a thermal vacuum or on a stand during vibration tests. The only requirement is, that the illumination of the test volume between the stimulator and the CHU can be dimmed to an extent that allows for star tracking (i.e. 0.001lux or less).

In the basic test setup, the stimulator is placed at a pre-specified distance from the lens of the CHU under test. This distance is typically 200mm, but may be as large as 2000mm, depending on the specific circumstances. When the proper distance has been verified, the laser-finder may be used to adjust the stimulator relative to the lens of the CHU. The microASC may now be turned on, and after issuing some specific test commands, it will recognize the star pattern of the stimulator, and the latter may be moved according to the test in progress. E.g. if a polarity test is called for, the stimulator may be turned relative to the spacecraft, successively, in each of the three degrees of freedom of the attitude.

The mechanical and optical stability of the stimulator is excellent, and biases less than 1 arcsecond are achievable over a time-span of tens of hours.

9.5 EGSE

The EGSE program supports the full tele-command and telemetry structure of the microASC. It might be used for a variety of purposes such as:

- Familiarisation with the command structure of the microASC.
- Support for checkout of the microASC functionality.
- Support for real sky verification and performance envelope of the instrument.
- Support for closed loop testing.
- Generation of upload commands.
- Upload of software updates.
- Upload of new parameter values.
- Debug dump device during system integration.
- Off-line operation of the instrument.
- Support for internal calibration measurements.
- Support for inter-calibration measurements.

Emphasis has been put on a logical structure and grouping of the commands. The program gives bounds for critical parameters and potential hazardous commands are double prompted.
The EGSE runs on a standard Microsoft Windows XP (or alternatively, Windows 98) PC.

10 Performance Envelope / Fact Sheet

Size:

Camera Head Unit:	50 x 50 x 57.5mm lens included (excl baffle).
microDPU:	Single: 100 x 75 x 41.2mm Double:124 x 100 x 41.5mm
Inner Baffle:	Depends on the envelope and the requirements
Outer Baffle:	Depends on the envelope and the requirements.

Mass:

Camera Head Unit:	260g incl. kinematic mount and 30kRad shielding, without harness.
microDPU:	Single: 310g including shielding to 30KRad Double: 570g including shielding to 30KRad
Inner Baffle:	Depends on the envelope and the requirements. A typical mass is 65g
Outer Baffle:	Depends on the envelope and the requirements. A typical mass is 400g

The following items shall also be considered in the mass budget:

- harness: 80g/m
- connectors 6g/set
- kinematic mount: 12g

Environs: The camera head requires low out-gassing environment during storage and launch. This is to prevent condensation on the lens.

Magnetic: Static magnetic moments: microDPU $< 5mAm^2$
CHU $< 0.05mAm^2$

Radiation: Each single IC component in the CHU has been TID-tested to survive at least 30 kRad(Si) of ionizing radiation first by a general screen-test and later from testing of samples from each lot of components. The Camera Head Unit is designed and tested to accept a lifetime dose of 30 kRad(Si). Internal shielding reduces this level so that less than 500 Rad(Si) is received by the CCD. All components in the CHU are also protected against SEL by current-monitoring LU-immune circuitry. No failure propagation on system level can thus occur due to transients. If a CHU experiences a LU, the latchup circuitry automatically resets the affected CHU only, returning the CHU to nominal operation after 4.3 seconds.

For the microDPU each single IC component has been TID-tested to survive 30 kRad(Si) of ionizing radiation, first by screen-test and later from testing of samples from each lot of components. Test samples (from Flight Lot) have been tested of each Lot demonstrating the homogeneity. The number of samples from the flight is 10-12. The standard Data Processing Unit is designed and tested to a lifetime dose of 30 kRad(Si). Internal shielding reduces this to less than 10 kRad.

All components in the microDPU are protected against SEL by current-monitoring latchup (LU) immune circuitry. In case a LU occurs, the microDPU is automatically power cycled and rebooted.
The Watchdog circuitry reboots the microASC in case of SEU in the CPU or SDRAM. All SDRAM, FLASH RAM, cache memory, and memory pipelines are protected by a Hamming code based EDAC that inline detects and corrects single bit SEUs and detects double bit errors. In case a double bit fault is detected, the unit will be automatically rebooted. No failure propagation on system level can thus occur due to SEUs.

At the beginning of 2005, the components in the microDPU were proton tested at the University Hospital of Copenhagen at 32 MeV. An additional proton test at 300 MeV was carried out in February 2006, in order to cover the range of high-energetic protons. These tests have been completed successfully.
Full tests for SEE sensitivity of the DPU and CHU IC components were performed at 7 HIT campaigns in 2006-2011. All components were tested up to the highest applicative LET. None of the tested components experienced any kind of permanent damage, i.e. all encountered phenomena were either recovered naturally or by power cycling. No reboot problems were encountered.

Vibration: The CHU has been vibration tested to comply with a variety of different mission specifications (see table at the end of this section). For the microDPU, the redundant unit has been tested at MECANO in Toulouse, France, to qualification level. For all components (microDPU, CHU, inner and outer baffle) the first resonance frequency is found above 140Hz.

Temperature: The data processing unit requires the box surface temperature to be between -40EC and +70EC. The camera head requires an operating temperature between -60EC and +20EC for maximum performance, but will operate at reduced accuracy up to +35EC. For all missions, a proper CHU operating temperature range has been achieved by passive radiation balance and heat storage.

Electrical data:

Voltage: The data processing unit accepts unregulated voltages from 17V to 64V. Voltages for the CHUs are generated in the microDPU. The power input is protected against inverse polarity connection and overcurrent.

Power: Nominal power consumption is 0.5W per CHU and 3.6W for the microDPU, resulting in a total nominal power consumption of 5.7W for a 4CHU configuration. The peak power consumption is 6.2W.

CHU 0.5W (part of the power consumption takes place inside the microDPU. From the thermal standpoint, the CHU dissipates only 0.27W)

Communication: Telemetry and telecommand comply with the Packet Utilization Standard (PUS) implementation of the CCSDS. The low-level protocol is a full duplex RS422, xon-xoff RTS/CTS and user selectable bits, rate (up to 115.2kbps) and parity. Debug and umbilical port may be set up as full redundant data port. Transmission support back to back transfer. Two dedicated differential lines are prepared for time synchronization.

EMC: Surpassing the MIL-STD-461C, MIL-STD-461D, MIL-STD-462D, MIL-STD-641F requirements.

Performance data:

Accuracy: Single image accuracy is better than 1 arcsecond 1Φ pointing and 8 arcsecond 1Φ roll. Further improvements based on an orbital model and multiple images are possible.

Update rate: For 1 full precision update per second the attitude latency is less than 1.1s. Time aperture jitter is less than 10:s, with respect to, e.g. GPS time. The update rate may by command be from 1/8 to 4Hz/CHU.

Autonomy: Auto system gain setting. Fast autonomous recovery from optical overloading. Autonomous recovery from lost in space in 80ms. Auto imaging with selectable compression. Auto non-stellar object tracking. Autonomous single-multiple CHU operation switching.

Star catalogue: Stellar positions based on a compilation of the Tycho and Hipparcos catalogues. The microASC catalogue contains the 14.000 brightest (CCD) stars. The microASC data base for initial attitude acquisition contains the 4000 brightest stars.

Warm-up time: Up to 6s for the microASC from power-on to issue full accuracy attitude measurements.

11 Product Assurance

11.1 Parts

Autonomous processes, as those used to implement the microASC, pose rather high demands to the performance level of the platform on which the processes are executed. This performance level inevitably leads to a system design of sizeable complexity, requiring the use of either large electronic circuit boards, or the use of highly integrated and high performance chips.
This, in turn, has led to an approach, where each device for the design is selected based on its merits of performance level, radiation tolerance, and power consumption, rather than relying on the comparatively low performance of devices listed in PPLs.

Indeed, by selecting device types with high functionality, the parts count is kept low, thereby increasing the overall reliability of the system. Furthermore, low power consumption also implies low operating temperatures and gentler thermal cycles hence enhancing the lifetime of the instrument.
This selection process has led to the choice of industrial or even commercial chips over class-s candidates.

The test program is performed in three steps:

- Components selection: to identify suitable chips
- Components acceptance I: to verify the quality of the purchased batch
- Components acceptance II: to check the proper operations and functionality, infant mortality etc.

Therefore, in order to assess the suitability of these components for space applications, the candidate chips are subjected to a thorough stress test program that includes thermal, mechanical, radiation (p+, e- and gamma), and electrical tests (details are given in "Parts Selection and Upscreening Procedure", ref. ASC-DTU-PR-3101). See appendix A for a comparison of the EEE-INST-002 and the way DTU upscreens and qualifies the components for space.

The Upscreening Procedure has been used since the first Star tracker for the ØRSTED satellite was designed and developed at the DTU in the 1990s. The number of tests used to qualify the components has been increased and below are listed some of the tests to qualify the Lot:

- TiD Testing
- X-Ray (screening according to MIL-STD-883F method 2012 and PEM-INST-001)
- Proton Testing (SEU & SEL. For RAM and CPU components also SEE)
- Heavy Ion Testing
- Destructive Physical Analysis (DPA)
- Microsection of PCB (according to IPC-6012B Class 3A)
- Accelerated Lifetime Test
- VTFMT (Voltage, Temperature, Frequency Margin Test, which is similar to WCA)
- Shock Test
- Shake Test
- Thermal Cycling

- Real Sky Testing

When the upscreening procedure for PEMs was developed at DTU, NASA developed in parallel an instruction for selection, screening and qualification of EEE Parts (311-INST-001, Aug. 1996), which was similar to the procedure developed at DTU.

To be able to assert a reliability measure with high confidence for a supposedly uniform lot of devices, an unpractical high number of devices must be tested when irradiating to a predefined dose level. However, applying the Overtesting Procedure, where the irradiation continues until functional failure, a reliability measure can be attained even for a small sample size [ASTM F 1263_94. "Standard Guide for Analysis of Overtest Data in Radiation Testing of Electronic Parts"]. This method is used for the upscreening of the components, and the number of samples from the Lot is usually between 4 and 12.

The capability of the components of the microASC to perform in the harsh space environment (radiation, temperature, vacuum) and their robustness have been verified and proven by several space flights covering extreme illumination, temperature, and radiation conditions.
The results from space also confirm thorough understanding of the physics of the environment, of the instrument that DTU has developed, and of their interaction. In addition, the results confirm adequacy of the methodology developed by DTU.

The Declared Components List (DCL) is already consolidated and compiled, and it is available upon request. The DCL is subject to configuration control.

All the components in the DCL belong to upscreened and flight qualified batches.

11.2 Materials

Materials and mechanical parts, which have successfully been used in space, are preferred. The Declared Materials List (DML) is already consolidated and compiled, and it is available upon request.

The DML is subject to configuration control.

Raw materials are accompanied by COC.

No forbidden materials have been used in the microASC (microDPU, CHU), baffles, and supporting equipment.

All materials are subject to thermal cycling. The test is performed on assembled and powered units, since it is more representative of the thermal loading and coupling.

Aluminium surfaces are treated for corrosion protection with space-approved chemical conversion coating (see DPL).

No limited lifetime materials are used in the microASC (microDPU, CHU) and baffles.

11.2.1 Outgassing

The outgassing properties of the materials are reported in the DML and DPL, and they are compliant with the ESA standards.

The TML of the complete instrument (microDPU, CHU and baffle) and its characterization have been determined by test. The test report may be available upon request.

11.2.2 Atomic Oxygen

The effects of the atomic oxygen are assessed on the basis of the orbital parameters and mission duration.

In order to avoid the erosion by the atomic oxygen, which may induce loss of performance, the baffle outer surface and knives are coated with a totally AO erosion resistant SiO_2 layer.

This special coating technique of CFRP structures was developed and has been verified in space onboard the CHAMP spacecraft.

AO erosion of the anti-reflex coating of the lens system is also a possibility. The microASC lens anti reflex coating is based on metal-dioxides known to have minimal AO sensitivity.

11.3 Processes

All the processes applied in the production of the microASC are compliant with the ESA ECSS-Q-ST-70C standards.
The Declared Process List (DPL) is already consolidated and compiled, and it is available upon request.

The DPL is subject to configuration control.

It is also important to stress that all the PCBs are populated by hand soldering. This process is performed by personnel, who are qualified and certified by ESA (soldering, welding, crimping, etc.).

11.4 Reliability

The reliability is defined as the probability that an instrument will function for at least a specified time.
The microASC reliability is established by statistical methods using the Failure-In-Time (FIT) number, which is the number of failures per 10^9 device-hours.

The microASC FIT numbers have been determined by performing accelerated life-time tests. For an in-orbit lifetime of 5 years, the reliability of the Star tracker is calculated by using the FIT number from the accelerated life-time tests of the CHU and microDPU, which shows that the Star Tracker is a very reliable instrument.

Units	FIT#	Reliability for at least one operational unit at EOL (Mission lifetime = 5 Years)
2 CHU	12 @ 0 degC	0.9999
Double microDPU	89 @ 20 deg C	0.9999

To insure the reliability of the microASC, all the components have been derated according to ECSS-Q-ST-30-11C, a FMECA has been made according to ECSS-Q-ST-30-02C, and a "Voltage Temperature Frequency Margin Test" has been performed (VTFMT is similar to WCA).

11.5 PA Activities

At DTU different PA activities have been implemented according to PA Plan [Ref.ASC-DTU-PL-3001], e.g. Non-Conformance Procedure, Cleanliness Contamination Control Procedure, Storage Procedure, and Configuration Control Procedure etc. The PA plan describes in more details all the PA activities, which are performed at DTU.